Extremophiles (2007) 11:481–493
DOI 10.1007/s00792-006-0060-z

ORIGINAL PAPER

# Thermal stability of isocitrate dehydrogenase from *Archaeoglobus fulgidus* studied by crystal structure analysis and engineering of chimers

**Runar Stokke · Mikael Karlström · Nannan Yang · Ingar Leiros · Rudolf Ladenstein · Nils Kåre Birkeland · Ida Helene Steen**

Received: 10 October 2006 / Accepted: 20 December 2006 / Published online: 31 March 2007


**Abstract** Isocitrate dehydrogenase from *Archaeoglobus fulgidus* (*Af*IDH) has an apparent melting temperature ($T_m$) of 98.5°C. To identify the structural features involved in thermal stabilization of *Af*IDH, the structure was solved to 2.5 Å resolution. *Af*IDH was strikingly similar to mesophilic IDH from *Escherichia coli* (*Ec*IDH) and displayed almost the same number of ion pairs and ionic networks. However, two unique inter-domain networks were present in *Af*IDH; one three-membered ionic network between the large and the small domain and one four-membered ionic network between the clasp and the small domain. The latter ionic network was presumably reduced in size when the clasp domain of *Af*IDH was swapped with that of *Ec*IDH and the $T_m$ decreased by 18°C. Contrarily, *Ec*IDH was only stabilized by 4°C by the clasp domain of *Af*IDH, a result probably due to the introduction of a unique inter-subunit aromatic cluster in *Af*IDH that may strengthen the dimeric interface in this enzyme. A unique aromatic cluster was identified close to the N-terminus of *Af*IDH that could provide additional stabilization of this region. Common and unique heat adaptive traits of *Af*IDH with those recently observed for hyperthermophilic IDH from *Aeropyrum pernix* (*Ap*IDH) and *Thermotoga maritima (Tm*IDH) are discussed herein.

**Keywords** Isocitrate dehydrogenase · *Archaeoglobus fulgidus* · Thermostability · Chimers

**Abbreviations**

| | |
|---|---|
| IDH | Isocitrate dehydrogenase |
| GDH | Glutamate dehydrogenase |
| *Ap*IDH | *Aeropyrum pernix* IDH |
| *Ec*IDH | *Escherichia coli* IDH |
| *Bs*IDH | *Bacillus subtilis* IDH |
| *Tm*IDH | *Thermotoga maritima* IDH |
| *Af*IDH | *Archaeoglobus fulgidus* IDH |
| *Pf*IDH | *Pyrococcus furiosus* IDH |
| $T_m$ | Melting temperature |

Communicated by G. Antranikian.

Enzyme EC number: (EC 1.1.1.42)

R. Stokke · N. K. Birkeland · I. H. Steen (✉)
Department of Biology, University of Bergen, PO Box 7800, Jahnebakken 5, 5020 Bergen, Norway
e-mail: Ida.Steen@bio.uib.no

M. Karlström · R. Ladenstein
Center for Structural Biochemistry, Department of Biosciences and Nutrition at Novum, Karolinska Institutet, 141 57 Huddinge, Sweden

N. Yang · I. Leiros
The Norwegian Structural Biology Centre (NorStruct), University of Tromsø, 9037 Tromso, Norway

## Introduction

Hyperthermophilic organisms are defined by a temperature optimum for growth at or above 80°C (Stetter 1999). All hyperthermophiles known so far are prokaryotes, although a few eukaryotic organisms, such as the Pompeii worm (*Alvinella pompejana*), have been found in the hot waters of hydrothermal vents where they experience a thermal gradient of 60°C or more over its body length (Cary et al. 1998).

Most of the hyperthermophilic microorganisms belong to the archaeal domain although hyperthermophiles have been found in the two bacterial orders, *Thermotogales* and *Aquificales* (Blöchl et al. 1995). Enzymes synthesized by (hyper)thermophiles are typically thermostable, or resistant to irreversible inactivation at high temperatures, and thermophilic, i.e. optimally active at elevated temperatures between 60 and 125°C (Vieille and Zeikus 2001). In order to reveal main adaptive strategies used for protein stabilization, numerous three-dimensional structures of hyperthermophilic proteins have been obtained. Comparative studies between hyperthermophilic and mesophilic enzymes have demonstrated that interactions such as hydrogen bonds, disulphide bonds, ion pairs, salt bridges, hydrophobic interactions and compactness are of importance for stability (Scandurra et al. 2000; Vieille and Zeikus 2001). No universal basis of stability has been recognized and the major reason for this is the relatively small free energy difference between the folded and the unfolded state and the complex way in which the small number of weak forces, determining protein stability, interplay with each other (Karlström et al. 2005). However, the most common determinants for increased thermal stability are in the first line a statistical prevalence of ionic interactions at the protein surface, increased formation of large ionic networks, electrostatic optimization and the reduction of repulsive charge–charge interactions (Spassov et al. 1997; Vetriani et al. 1998; Karshikoff and Ladenstein 2001; Karlström et al. 2005). Despite a great availability of data on thermophiles and thermophilic proteins, most of the information generated on how proteins from hyperthermophilic organisms have adapted in their natural environments are based on case studies (Karshikoff and Ladenstein 2001) or structural and biochemical comparisons of single mesophilic/hyperthermophilic enzyme pairs.

We have chosen the enzyme isocitrate dehydrogenase (IDH) as a model enzyme for studying environmental adaptations of proteins to extreme temperatures. IDH catalyses the oxidative decarboxylation of D-isocitrate to 2-oxoglutarate and $CO_2$ with $NAD^+$ (EC 1.1.1.41) or $NADP^+$ (EC 1.1.1.42) as cofactor and comprises a diverse enzyme family with regard to cofactor specificity, primary structure, and oligomeric state.

*Aeropyrum pernix* (*Ap*), *Pyrococcus furiosus* (*Pf*), *Archaeoglobus fulgidus* (*Af*) and *Thermotoga maritima* (*Tm*) are hyperthermophilic microorganisms growing optimally at 95, 100, 83 and 80°C, respectively (Fiala and Stetter 1986; Huber et al. 1986; Sako et al. 1996). We have previously estimated the thermal stability of *Ap*-, *Pf*-, *Af*- and *Tm*IDH by determination of the apparent melting temperatures ($T_m$) using differential scanning calorimetry (DSC) (Steen et al. 2001). It was found that *Ap*IDH has highest thermal stability with a $T_m$ of 109.9°C. *Pf*, *Af* and *Tm*IDH were less stable with a $T_m$ of 103.7, 98.5, and 98.3°C, respectively. However, each of the hyperthermophilic IDHs showed a significantly higher $T_m$ than the one determined for IDH from *Escherichia coli* ($T_m$ = 52.6°C) (*Ec*IDH) (Karlström et al. 2005) and pig ($T_m$ = 59°C) (Karlström et al. 2006). Recently, the three-dimensional structures of *Ap*IDH (Karlström et al. 2005) and *Tm*IDH (Karlström et al. 2006) have been resolved and the structural properties important for their high thermal stability have been identified.

Here we report the crystallization and structure determination of the hyperthermophilic *Af*IDH including a comparative structural study with other known IDH homologs. Furthermore, chimers between the hyperthermophilic *Af*IDH and the mesophilic *Ec*IDH were constructed to investigate the contribution of the clasp domain to the thermal stability of wild-type *Af*IDH.

## Materials and methods

### Strains

*Escherichia coli* strain EB106 (*icd*-11 *dadR*1 *trpA*62 *trpE*61 *tna*-5 *lambda*$^-$) was originally obtained from the *E. coli* Genetic Stock Centre, MCD Biology Department, Yale University, in courtesy of Dr. Mary K.B. Berlyn. In order to express proteins in this strain, *E. coli* EB106 was lysogenized using the λDE3 Lysogenization Kit from NOVAGEN.

### Crystallization and data collection

*Af*IDH was crystallized using the hanging drop vapour diffusion technique with reservoir solution consisting of 0.6 M $ZnSO_4$ and 0.1 M Na Cacodylate, pH 6.3, which are optimized from the Nextal EasyXtal Cations suite condition number 60 (QIAGEN GmbH, Hilden, Germany). Crystals were grown by mixing equal volumes (2 µl) of a 9 mg/ml protein solution with the reservoir solution. The drops were equilibrated at 8°C. 20% (v/v) glycerol added to the reservoir solution sufficed as a cryo-protectant for flash-cooling the crystals in liquid nitrogen. A data set (see Table 1) was collected at the macromolecular crystallography beamline X06SA at the Swiss Light Source (SLS). The

**Table 1** Data collection and refinement statistics for *Af*IDH

| | |
|---|---|
| Data collection | |
| Wavelength (Å) | 0.92 |
| Space group | $P2_1$ |
| Unit cell parameters (Å, °) | 81.6, 65.4, 87.2, 90, 95.28, 90 |
| Resolution range (Å) | 40–2.5 (2.64–2.5) |
| No. observed reflections | 130993 (19123) |
| No. unique reflections | 31867 (4612) |
| Redundancy | 4.1 (4.1) |
| Completeness (%) | 99.8 (100.0) |
| Mean I/$\sigma$I | 11.1 (3.5) |
| $R_{merge}$ (%) | 11.4 (47.6) |
| Refinement | |
| Non-hydrogen atoms | 6553 |
| Metal ions | 9Zn/3Cl |
| No. solvent molecules | 94 |
| Overall B-factor (Å$^2$) | 16.80 |
| $R_{cryst}$ (%) | 19.6 |
| $R_{free}$ (%) | 25.4 |
| Deviation from ideal geometry | |
| Bond lengths (Å) | 0.016 |
| Bond angles (°) | 1.785 |
| Ramachandran plot | |
| Most favoured region (%) | 87.7 |
| Allowed regions (%) | 11.7 |
| Disallowed regions (%) | 0.6 |

data were collected with a MAR225 CCD detector and allowed the determination of the crystal structure using molecular replacement techniques.

## Structure determination and refinement

The collected data set was indexed and integrated using MOSFLM (Leslie 1992). The crystals were monoclinic, with unit cell parameters of $a$ = 81.6 Å, $b$ = 65.4 Å, $c$ = 87.2 Å, $\beta$ = 95.28°. The data were scaled, merged and the intensities were converted into structure factors using the CCP4 programs SCALA and TRUNCATE (CCP4 1994). A summary of the data collection statistics is presented in Table 1. The systematic absences in the collected data set indicated the presence of a twofold screw axis along the b-axis, with the only possible space group being $P2_1$. The solvent content was estimated to be around 52%, with a Matthews Coefficient of 2.6 Å$^3$ Da$^{-1}$, assuming two protein molecules per asymmetric unit. The crystal structure of *Af*IDH was determined by molecular replacement methods using MOLREP (CCP4 1994). The crystal structure of *Ap*IDH was used as search model and the automated program functions in MOLREP were applied in order to create the model that presumably had the best fit to the sequence of *Af*IDH. Reflections up to a high-resolution limit of 3.5 Å were used. One well-resolved solution for the two molecules in the asymmetric unit could be found, having a correlation coefficient of 0.459 and an $R_{factor}$ of 45.1%. A rigid-body fitting of the model using a high-resolution cut-off at 2.5 Å resulted in $R_{work}$ of 44.5% ($R_{free}$ of 46.0%). After a manual intervention using O (Jones et al. 1991), the model was refined in REFMAC5 (Murshudov et al. 1999), resulting in $R$-factors of 24.0 and 29.1% for the working and test sets of reflections, respectively. Subsequent cycles of refinement interspersed with manual rebuilding, gave final $R_{work}$ and $R_{free}$ values of 19.6 and 25.4%, respectively, with acceptable protein geometry. In general, water molecules were added using the embedded functions found in REFMAC and manually checked using O. The four residues found in disallowed regions of the Ramachandran plot are all located in flexible loops.

## Structure analysis

Sequence alignment was performed using the program STAMP (Russell and Barton 1992) based on the $C^{\alpha}$-atom coordinates and secondary structural assignments using the program DSSP (Kabsch and Sander 1983). Potential salt-bridge formation and ionic networks were analysed using the program CONTACT (CCP4 1994) and IONSTAT (W. Meining, unpublished) with varying maximum distances from 3.5 to 8.0 Å. Accessible surface areas were calculated using CNS with Ala, Ile, Leu, Met, Phe, Pro, Trp, and Val defined as hydrophobic residues, Asn, Gln, Ser, Thr, Tyr, Cys and Gly regarded as polar residues and Asp, Glu, Arg, Lys and His as charged residues. The water probe radius was set to 1.4 Å and the accuracy of the numerical integration was set to 0.12. Water and ions were excluded from the model.

## Figure preparations

Figures 1, 3, 4 and 5 were made using the program PYMOL (PyMol 2005) and Fig. 2 was prepared using the program ESPript2.2 (Gouet et al. 1999).

## Cloning and engineering of chimers

The wild-type *Ec idh* gene was amplified from *E. coli* K12 (DSMZ - Literature Reference No. 4684) genomic DNA by PCR using the primers P1-P2 (Table 2) and ligated into pET101/D-TOPO (Invitrogen Corporation, Carlsbad, CA 92008, USA). Domain-swapping of the clasp domain from *Ec*IDH with the clasp domain from *Af*IDH was performed by using the ExSite$^{TM}$PCR-Based Site-Directed Mutagenesis Kit (Stratagene, La Jolla, CA, USA) with the pET101/D-TOPO-*Ec idh* as

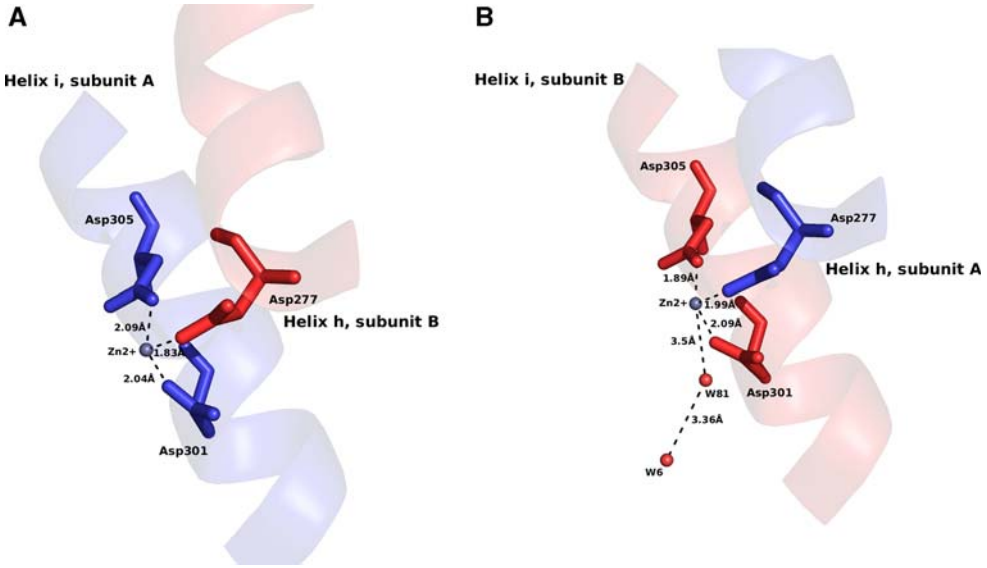


**Fig. 1** The structure of *Af*IDH was crystallized and resolved without substrate and cofactor in the active site, however, a high concentration of zinc was present in the crystallization condition. A zinc ion was found tightly bound to *Asp301*, *Asp305*, *Asp277′* in the active site of subunit A (**a**) and subunit B (**b**) of *Af*IDH. Amino acids from subunit A are coloured *blue* and amino acids from subunit B are coloured *red*. Amino acids from both subunits are involved in binding of zinc

template. Mutagenesis was performed as described in the manufacturer protocol. Because of the large size of the mutagenic primers the mutagenesis was performed in a two-step reaction with primers P3-P6 (Table 2). Swapping of the clasp domain from *Af*IDH with the clasp domain from *Ec*IDH (*Af*IDH/*Ec*IDH$_{clasp}$) was

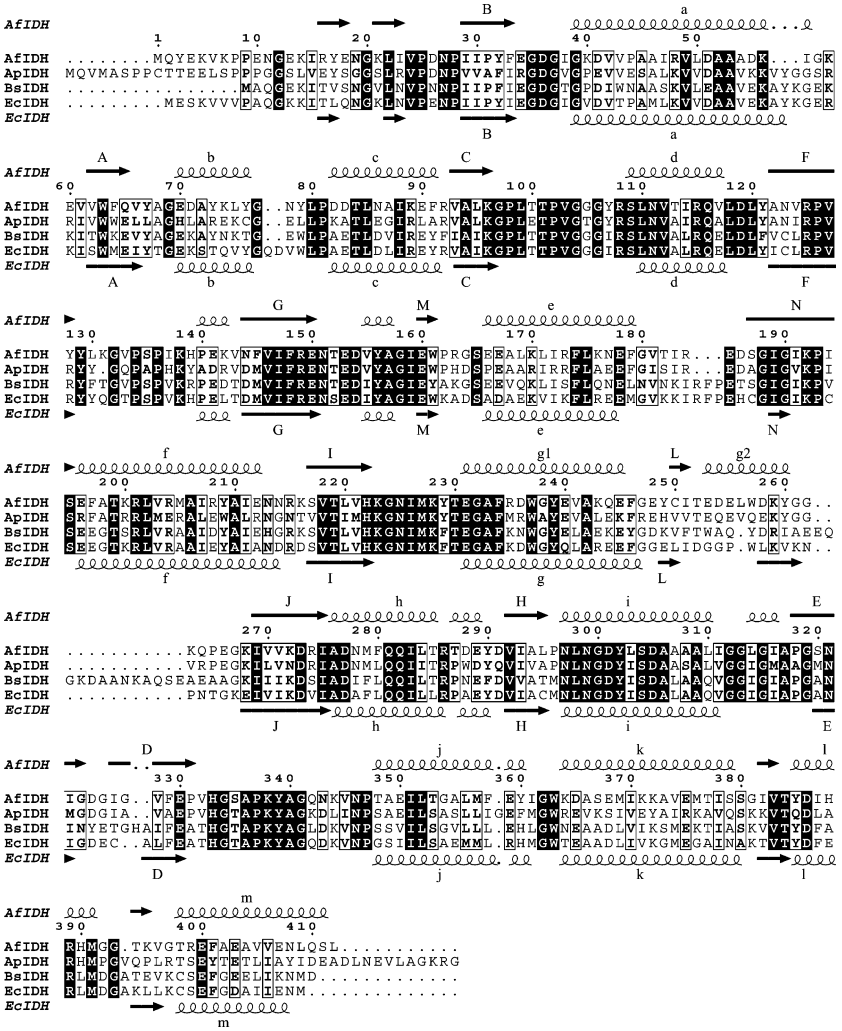


**Fig. 2** Sequence alignment of *Af*IDH, *Ap*IDH (PDB code 1TYO), *Bs*IDH (PDB code 1HQS) and *Ec*IDH (PDB code 1SJS) with the secondary structure elements of *Af*IDH (*top*) and *Ec*IDH (*bottom*). Identical and similar residues are *boxed*. The secondary structure elements were given the nomenclature as implemented in *Ec*IDH (Hurley et al. 1989) and the figure was made in ESPript2.2 (Gouet et al. 1999)

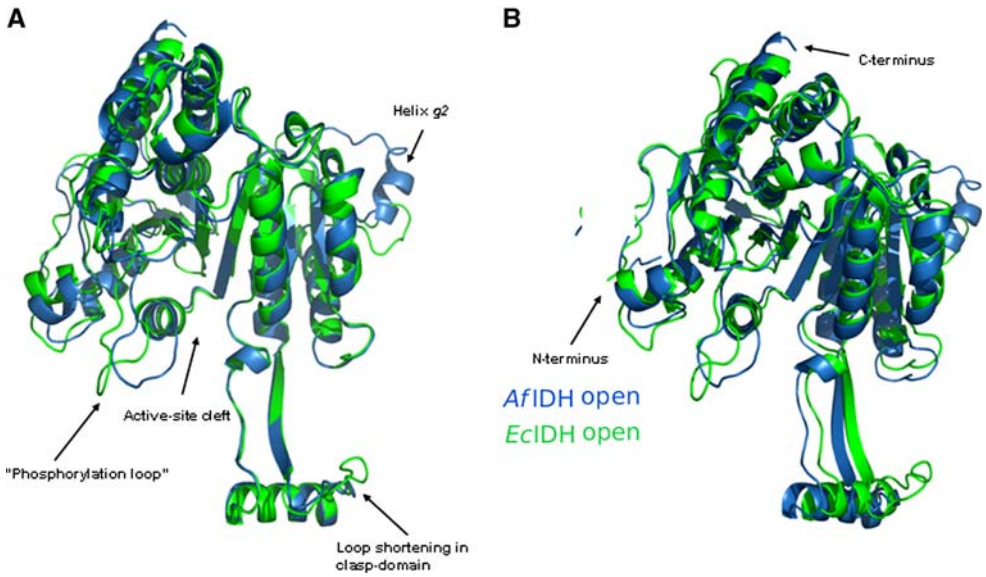


**Fig. 3** Overlay of the small (**a**) and large (**b**) domains of *Af*IDH and *Ec*IDH$_{open}$

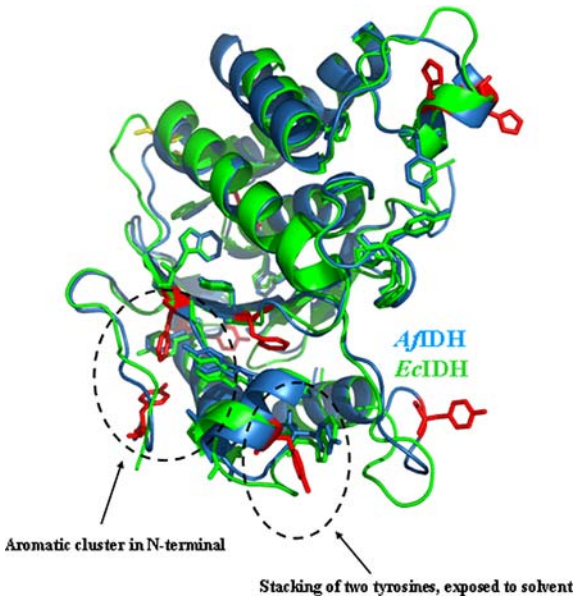


**Fig. 4** Overlay of large domain from *Af*IDH and *Ec*IDH showing the difference in aromatic residue content in the N-terminus. *Red* and *blue*; *Af*IDH (Tyr3, Phe64 and Phe91), *green*; *Ec*IDH (Tyr95)

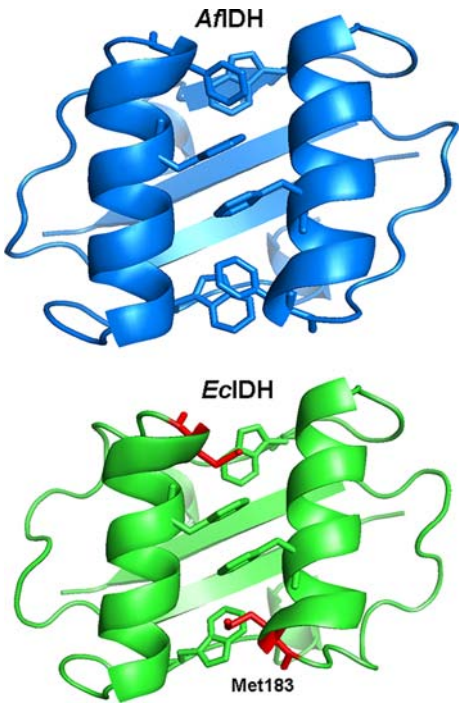


**Fig. 5** Clasp domain from *Af*IDH (*blue*) and *Ec*IDH (*green*) showing an aromatic cluster in the *Af*IDH structure compared to *Ec*IDH. *Ec*IDH contained a Met residue (*red*) in the corresponding position of Phe179 in *Af*IDH

performed by overlap extension PCR (Warrens et al. 1997) on the template pET-11-a/*Af idh* (Steen et al. 2001) using primers P7-P14 (Table 2). For expression, the chimer construct was sub-cloned into pET101/D-TOPO vector using primers P15-P16 (Table 2) to amplify the gene.

## Expression and purification

Expression and purification of wild-type *Af*IDH and *Af*IDH/*Ec*IDH$_{clasp}$ were performed as previously described for wild-type *Af*IDH (Steen et al. 2001). Expression of wild-type *Ec*IDH and *Ec*IDH/*Af*IDH$_{clasp}$ was performed at 37°C in *E. coli* strain EB106 (DE3) in LB broth containing ampicillin (100 μg/ml). Isopropyl-*β*-thiogalactopyranoside was added to 1.0 mM concentration to induce expression at $A_{600\ nm}$ = 0.7–0.8, and the incubation was

**Table 2** Primers used for construction of wild-type *Ec idh* and chimeras

| Name | Primer sequence | Product |
|---|---|---|
| P1 | 5′-caccatggaaagtaaagtagttgttc-3′ | Wild-type *Ec idh* (K12) in pET101/D-TOPO |
| P2 | 5′-cattacatgttttcgatgatcgcg-3′ | |
| *Step 1* | | *Ec idh*/*Af idh* in pET101/D-TOPO |
| P3 | 5′-gacgtgtacgccggtatagagtggcctcatgacagccctgaggctgcgaggattaggagg ttcctgcgtgaagagatg-3′ | |
| P4 | 5′P-ttccgagttttcacggaagataacc-3′ | |
| *Step 2* | | |
| P5 | 5′-ttcctcgcagaggagttcgggatatcgataagggaggacgccggcatagggttaagccg tgttcggaagaaggc-3′ | |
| P6 | 5′P-cctcctaatcctcgcagcctcagg-3′ | |
| P7 | 5′-cgcataaatgtcttcggtgttctccctgaaaataacg-3′ | *Af idh*/*Ec idh* by overlap extension PCR |
| P8 | 5′-gagaacaccgaagacatttatgcgggtatcgaatgg-3′ | |
| P9 | 5′-aaactcgctgatcggcttaataccgataccacaatgttc-3′ | |
| P10 | 5′-ggtattaagccgatcagcgagtttgccaccaagag-3′ | |
| P11 | 5′-ccagtagcgctcgaaggagagg-3′ | |
| P12 | 5′-cattacatgttttcgatgatcgcg-3′ | |
| P13 | 5′-acacaagcttgaaggagatatacatatgcagtacgagaaggtcaaacctcc-3′ | |
| P14 | 5′-caggatcctcatagcgactgcaggttttcaacc-3′ | |
| P15 | 5′-caccatgcagtacgagaaggtcaaacctcc-3′ | *Af idh*/*Ec idh* in pET101/D-TOPO |
| P16 | 5′-caggatcctcatagcgactgcaggttttcaacc-3′ | |

continued for 4–5 h at 37°C. Cells were harvested by centrifugation (5000×*g* for 15 min) and frozen at –20°C until used. Cells carrying expressed wild-type *Ec*IDH or *Ec*IDH/*Af*IDH$_{clasp}$, were resuspended in 20 mM sodium-phosphate buffer, pH 7.0, containing 1 mM EDTA and disrupted using a French pressure cell. After removal of cell debris by centrifugation (10,000×*g* for 30 min) the cell extracts were applied to a Red Sepharose column (Millipore) equilibrated with 20 mM sodium phosphate buffer, pH 7.0 containing 1 mM EDTA. The column was first washed with the sodium phosphate buffer until $A_{280}$ was zero and then washed with the sodium-phosphate buffer containing 0.25 mM $NADP^+$. Protein was eluted with 20 mM sodium phosphate buffer, pH 7.0 containing 1.0 mM EDTA, 0.25 mM $NADP^+$, 10 mM isocitrate and 10 mM $MgCl_2$. Purified enzymes were stored in 20 mM Tris/HCl, pH 7.5, 50% glycerol and 1.0 mM DTT at –20°C.

## Temperature dependence and thermal stability

Thermal inactivation experiments were performed at 50°C for wild-type *Ec*IDH and *Ec*IDH/*Af*IDH$_{clasp}$ and at 65 and 70°C for wild-type *Af*IDH and *Af*IDH/*Ec*IDH$_{clasp}$. The 150 µl incubation solution contained 20 mM Tris/HCl, pH 7.5, 50% glycerol, 1.0 mM DTT and 3 µg of enzyme. Samples were collected at given times and remaining activity was measured using assays for the respective enzymes.

Differential scanning calorimetry was carried out with a VP-DSC MicroCalorimeter (MicroCal$^{TM}$). The samples were dialysed against the reference buffer (50 mM potassium-phosphate buffer, pH 7.5, 0.1 M NaCl). A protein concentration of 1.2 mg/ml was used for all enzymes. The calorimetric scans were carried out between 20 and 120°C for wild-type *Af*IDH and *Af*IDH/*Ec*IDH$_{clasp}$ and between 20 and 90°C for wild-type *Ec*IDH and *Ec*IDH/*Af*IDH$_{clasp}$ with a scan rate of 1 K/min. A second scan was run to estimate reversibility. Apparent $T_m$s were determined from the transition midpoint upon unfolding, due to the irreversible nature of the enzymes.

## Enzyme assay and measurement of kinetic properties

Enzyme activity of IDH was measured photometrically at 40°C (wild-type *Ec*IDH and *Ec*IDH/*Af*IDH$_{clasp}$) or 60°C (wild-type *Af*IDH and *Af*IDH/*Ec*IDH$_{clasp}$) by monitoring the formation of NADPH at 340 nm ($\varepsilon_{340}$ = 6.22 $mM^{-1}$ $cm^{-1}$). The 1 ml reaction contained 50 mM Tricine–KOH, pH 8.0 and 10 mM $MgCl_2$ at assay temperature, 1 mM isocitrate for wild-type *Ec*IDH and *Ec*IDH/*Af*IDH$_{clasp}$ or 3 and 5 mM for wild-type *Af*IDH and *Af*IDH/*Ec*IDH$_{clasp}$, respectively. Cofactor was added at a concentration of 0.25 mM. One Unit of enzyme activity is referred to as the reduction of 1 µmol of $NADP^+$ per minute. For determination of $K_m$ and $V_{max}$ values for isocitrate, the $NADP^+$ concentration was kept fixed at 0.25 mM while varying the isocitrate concentration. For determination of $K_m$ values for $NADP^+$, the isocitrate concentration was kept fixed at 1 mM for *Ec*IDH and *Ec*IDH/

*Af*IDH$_{clasp}$, 3 mM for *Af*IDH and 5 mM for *Af*IDH/*Ec*IDH$_{clasp}$ while varying the cofactor concentration. Kinetic data were analysed by the Direct linear plot using the Enzpack 3 software package (Biosoft, Cambridge, UK). Protein concentrations were measured by the method of Bradford (1976).

## Results and discussion

### Quality and description of the model

The final model of *Af*IDH comprises all 412 amino acid residues for both molecules in the asymmetric unit, although some side-chains are rather poorly defined in electron density. In addition, 9 Zinc atoms, 3 Chloride atoms and 94 water molecules were modelled in electron density. The final model and structure factors have been deposited in the Protein Data Bank with accession code PDB2IV0. For an overview of the refinement statistics, see Table 1.

### Overall structure and active site of *Af*IDH

As observed for all other IDHs, *Af*IDH consists of three domains; a large domain, a small domain and a clasp domain. Residues 1–120 and 312–412 belong to the large domain, residues 121–153 and 196–311 form the small domain and the remaining residues 154–195 form the clasp-like domain. *Af*IDH formed a homodimer in the crystal structure and the inter-subunit relationship and interface contacts in *Af*IDH are similar to those in other reported IDH structures (Hurley et al. 1989; Singh et al. 2001; Karlström et al. 2005). Apart from the formation of the clasp domain, the dimer associates through helices *h* and *i* in both subunits creating a stable four helix bundle.

The dimer has two active sites that are located in a deep cleft formed by the large and the small domains of one subunit and the small domain of the adjacent subunit. *Af*IDH was crystallized and its structure solved without substrate and cofactor in the active site, however two $Zn^{2+}$-ions were found tightly bound to Asp301, Asp305, Asp277′ (the prime indicates the second subunit) in the active site of both subunits (Fig. 1a, b). In subunit B a water molecule (W81) was also found in contact with $Zn^{2+}$ (Fig. 1b). In both *Ec*IDH and *Ap*IDH binding of $Ca^{2+}$ has been shown to involve conserved water molecules together with three conserved aspartic residues equivalent to those found in *Af*IDH (Stoddard et al. 1993; Karlström et al. 2005). Furthermore, *Af*IDH shares the highly conserved residues involved in substrate binding and catalysis as shown for *Ap*IDH, *Ec*IDH and *Bacillus subtilis* IDH (*Bs*IDH) (Dean 1993; Singh et al. 2001; Karlström et al. 2005) (Fig. 2). Thus, it is believed that *Af*IDH has similar interactions with substrate and cofactor in the active site. To this date several crystal structures of different $NADP^+$-dependent homo-dimeric IDHs have been reported: *Ec*IDH (Hurley et al. 1989) (PDB-codes 3ICD; closed form and 1SJS; open form), *Ap*IDH (Karlström et al. 2005) (PDB-codes 1XGV, 1TYO and 1XKD), *Bs*IDH (Singh et al. 2001) (PDB-code 1HQS), porcine heart mitochondrial IDH (Ceccarelli et al. 2002) (*Pc*IDH, PDB-code 1LWD), human cytosolic IDH (Xu et al. 2004) (*Hc*IDH, PDB-code 1T0L; closed form and 1T09; open form) and *Tm*IDH (Karlström et al. 2006) (PDB-code 1ZOR). Overlay structure analysis of *Af*IDH with other resolved structures of IDH revealed that it was most similar to *Ec*IDH. A comparison with the open and closed form of *Ec*IDH revealed *Af*IDH as more similar to that of the open conformation [root-mean-square distance (RMSD) of 0.99 Å] than to the closed conformation (RMSD of 1.78 Å). The RMS difference between the small domain and large domain of *Af*IDH versus that of the open structure of *Ec*IDH was 0.57 Å (using 170 $C^{\alpha}$-atoms) and 0.96 Å (using 208 $C^{\alpha}$-atoms), respectively (Fig. 3a, b). Secondary structure elements were given the nomenclature as implemented in *Ec*IDH (Hurley et al. 1989).

Overall, helix and strand regions were conserved in *Af*IDH compared to *Ec*IDH, however, some local differences were observed in *Af*IDH. An alignment based on secondary structural assignment (Fig. 2) revealed that a helix, *g2*, replaced the loop between strand *L* and strand *K* in *Af*IDH compared to *Ec*IDH. This *g2* helix has previously been observed in the structure of *Ap*IDH (Karlström et al. 2005).

### Thermal stability

The $\Delta T_m$ between *Ec*IDH and *Af*IDH is 45.4°C. As *Af*IDH showed highest structural similarity to *Ec*IDH, a comparative study was performed between these enzymes to reveal heat adaptive traits in the hyperthermophilic enzyme.

### Accessible surface area (ASA)

Analysis of *Af*IDH shows a significant increase of ASA contributed by polar residues and also a significant decrease of ASA contributed by hydrophobic residues compared to *Ec*IDH. However, the percentage of ASA contributed by charged residues was slightly lower in *Af*IDH compared to *Ec*IDH, which is also the case for the hyperthermophilic *Ap*IDH (Karlström et al. 2005).

The distribution of hydrophobic, polar and charged surface area of *Af*IDH and *Ec*IDH is shown in Table 3. The dimer interface of *Af*IDH buried 5,564 Å$^2$ of the 37,970 Å$^2$ molecular surface area (MSA) of the dimer, giving a solvent-accessible surface area of 32,406 Å$^2$ for the dimer. In contrast, the *Ec*IDH dimer buries 6,020 Å$^2$ of the 38,547 Å$^2$ of the dimer with a total solvent-accessible surface of 32,527 Å$^2$, i.e the buried inter-subunit surface comprise 14.7 and 15.6% of *Af*IDH and *Ec*IDH, respectively.

## Amino acid composition

The *Af*IDH subunit is made up of 412 amino acids of which 30.1% are polar residues, 27.2% charged residues and 42.7% hydrophobic residues. Compared to *Ec*IDH, the distribution of amino acids was similar in the two proteins with a slightly higher fraction of polar residues in *Af*IDH and a slightly higher fraction of hydrophobic residues in *Ec*IDH (Table 3). However, *Af*IDH has a significantly higher fraction of aromatic residues of 11.2% compared to 8.7% in *Ec*IDH. It has previously been shown that *Af*IDH and other archaeal hyperthermophilic IDHs have a decreased number of Cys residues compared with *Ec*IDH, 0.20 and 1.40%, respectively (Steen et al. 1997, 2001), hence, following the trend observed for thermophilic proteins whereby Cys residues tend to be avoided.

## Ionic interactions

Comparative studies between hyperthermophilic and mesophilic homologs have shown a clear tendency for the total number of ion pairs and large ionic networks to increase with the optimal growth temperature of the organisms as well as with the $T_m$ of the proteins (Yip et al. 1995, 1998; Knapp et al. 1997). Surprisingly, few differences were found between the mesophilic *Ec*IDH and the hyperthermophilic *Af*IDH in the total amount of charges and ionic interactions. The number of ionic networks at different cut off distances, are summarized in Table 3. Overall, the number and size of ionic networks did not differ significantly between *Af*IDH and *Ec*IDH; however, the location of the ionic networks seems to play an important role for the increased thermal stability of the hyperthermphilic enzyme. In

**Table 3** Characteristics of *Af*IDH and *Ec*IDH

| | *Af*IDH | *Ec*IDH$_{open}$ |
|---|---|---|
| PDB code | 2IVO | 1SJS |
| $T_m$ (°C) | 98.5 | 52.6[a] |
| Resolution (Å) | 2.5 | 2.4 |
| RMSD (Å) $C_\alpha$-atoms small domain/large domain/overall | 0.57/0.96/0.99 (170 atoms/208 atoms/378 atoms) | |
| RMSD (Å) $C_\alpha$-atoms of clasp-domain | 4.42 (total domain)/0.69 (without loop) (42 atoms/40 atoms) | |
| No. residues per subunit | 412 | 416 |
| Charged residues (%)[b] | 27.2 | 27.2 |
| Polar residues (%)[c] | 30.1 | 28.6 |
| Hydrophobic residues (%)[d] | 42.7 | 44.9 |
| Aromatic residues (%)[e] | 11.2 | 8.7 |
| No. ion pairs per dimer (4/6/8 Å)[f] | 53/104/175 | 58/110/181 |
| No. ion pairs per residue in dimer (4/6/8 Å) | 0.129/0.252/0.425 | 0.139/0.264/0.435 |
| Volume (×10$^4$ Å$^3$) | 8.5 | 8.4 |
| Accessible surface area of dimer (Å$^2$) | 32406 | 32527 |
| Buried inter-subunit surface (% of MSA) | 14.7 | 15.6 |
| No. residues forming two ion pairs (4/6/8 Å) | 14/41/60 | 18/50/75 |
| No. residues forming three ion pairs (4/6/8 Å) | 0/10/42 | 0/6/22 |
| No. 2/3/4 membered intra-subunit networks (4 Å) | 27/8/0 | 24/12/0 |
| No. 2/3/4 membered inter-subunit networks (4 Å) | 0/2/2 | 0/2/2 |
| % of charged residues forming ion pairs (4/6/8 Å) | 46/78/92 | 45/76/89 |
| Distribution of hydrophobic/polar/charged residues at accessible surface (%) | 20.7/30.1/49.3 | 25.6/23.1/51.3 |
| Distribution of hydrophobic/polar/charged residues at interface (%) | 47.0/27.3/25.7 | 50.4/19.7/29.9 |

*MSA* molecular surface area

[a] Data from Karlström et al. (2005)

[b] Charged residues: R, K, H, D, E

[c] Polar residues: G, S, T, Y, N, Q, C

[d] Hydrophobic residues: A, V, L, I, W, F, P, M

[e] Aromatic residues: W, F, Y, H

[f] Å cutoff

*Af*IDH, a three-membered inter-domain network was found at 4.0 Å cut off between Asp119 (helix *d*, large domain), Arg201 (helix *f*, small domain) and Asp324 (loop region between *β*-strand *E* and *D*, large domain). Although the amino acids involved in this network are conserved in *Ec*IDH, only a single ion pair was found in the mesophilic enzyme at 4.0 Å cut off distance. These amino acids are also conserved in *Ap*IDH and part of a seven-membered ionic network. Furthermore, a four-membered ionic network in *Af*IDH between the clasp domain, Arg163 (loop in clasp domain), and the small domain of the second subunit, Glu196′ (helix *f*), Lys200′ (helix *f*) and Glu240′ (helix *g1*), was observed as low as 3.5 Å cut off distance, hence, making this a possible strong salt–bridge interaction. No ionic network was observed in the clasp domain of *Ec*IDH with a 3.5 Å cut off, however, a three-membered ionic network was observed when analysed at 4.0 Å cut off. Hence, a stronger ionic contribution to stability may be present in the clasp domain of *Af*IDH compared to *Ec*IDH.

## Loop shortening

Shortening of small loops was observed in *Af*IDH compared to *Ec*IDH: by three residues in the loop between helix *a* and strand *A*; two residues between helix *b* and *c* and finally, three residues between helix *e* and strand *N* in the clasp domain (Figs. 2, 3). The two latter loop deletions were also reported in the structure of *Ap*IDH. Loop deletion or loop shortening is often seen in hyperthermophilic proteins and in many cases reflected by a higher content of secondary structure elements. Loop regions and random coil structures, particularly in solvent-exposed regions are usually flexible areas and most likely to collapse at elevated temperatures. Hence, loop–loop stabilization by ionic interactions can be crucial for maintaining the functional structure at high temperatures. In *Af*IDH, two loop–loop interactions were observed in each subunit closer than 4.0 Å: subunit A; Asp26-Lys59 (3.65 Å) and Arg215-Asp291 (2.64 Å), subunit B; Asp26-Lys59 (3.06 Å) and Lys216-Glu266 (3.0 Å). In *Ap*IDH, one loop–loop interaction was observed in each subunit equivalent to Asp26-Lys59 in *Af*IDH: subunit A; Asp34-Arg70 (3.73 Å), subunit B; Asp34-Arg70 (3.88 Å). However, no loop–loop interactions were observed in the mesophilic *Ec*IDH.

## Aromatic clusters

The presence of aromatic clusters has earlier been suggested to contribute to thermal stability of proteins (Kannan and Vishveshwara 2000; Dalhus et al. 2002). A large number of aromatic residues were observed in the N-terminus of *Af*IDH compared to *Ec*IDH (Fig. 4). An aromatic cluster of three residues; Tyr3 (N-terminus), Phe64 (*β*-strand *A*) and Phe91 (helix *c*), was observed in this region and is likely to protect the N-terminus from thermal unfolding. In the clasp domain of *Af*IDH, the conserved aromatic interaction between Phe174 and Phe174′ [in subfamily I IDHs (Steen et al. 2001)] on helix *e* was extended to an aromatic cluster by Phe179 and Phe179′ on helix *e* which, in addition involved Trp161 and Trp161′ on strand *M*, resulting in a six-residue aromatic cluster (Fig. 5). The aromatic cluster in the clasp domain has previously been observed in *Ap*IDH and is believed to provide stabilization of the interface. In *Ec*IDH, Phe179 in *Af*IDH is substituted with Met183.

## Stability effects in engineered chimers

Three features likely to contribute to the higher thermal stability in *Af*IDH *contra* *Ec*IDH were identified in the clasp domain; an aromatic cluster, a four-membered ionic network from both subunits to the small domain of the other subunit and a loop shortening; Lys186-Phe190 (*Ec*IDH numbering). In order to investigate the implications of these features on the thermal stability of *Af*IDH, chimeric proteins between *Af*IDH and *Ec*IDH were constructed. Each of the two chimers was composed of the large and small domain from one enzyme with the clasp domain from the second enzyme (*Ec*IDH/*Af*IDH$_{clasp}$ and *Af*IDH/*Ec*IDH$_{clasp}$). The presence of an aromatic cluster and a loop-shortening could be formed in the chimer *Ec*IDH/*Af*IDH$_{clasp}$ since these are present in the *Af*IDH-clasp**.** However, the four-membered ionic network cannot be formed since the network is not conserved in *Ec*IDH. Thus, a possible increase in stability of this chimera would be related to the formation of these two factors. In the chimer *Af*IDH/*Ec*IDH$_{clasp}$, a likely decrease in stability would be addressed to the removal of all three putative stabilizing factors mentioned above.

$T_m$ of the chimers was monitored by DSC and was as previously observed for the wild-type enzymes (Steen et al. 2001; Karlström et al. 2005) an irreversible process. A considerable decrease in $T_m$ was observed for the chimer *Af*IDH/*Ec*IDH$_{clasp}$ ($\Delta T_m$ – 18°C) as compared to wild-type *Af*IDH, followed by a reduction in half-life ($t_{1/2}$) and a lower apparent temperature optimum ($T_{opt}$) (Table 4). In contrast, swapping the *Af*IDH clasp into the *Ec*IDH increased

**Table 4** Thermal properties of chimers and wild-type IDH

| Enzyme | $T_m$ (°C) | $t_{1/2}$ (min) | $T_{opt}$ (°C) |
|---|---|---|---|
| *Ec*IDH | 52.6[a] | 24.2 (at 50°C) | 50 |
| *Ec*IDH/*Af*IDH$_{clasp}$ | 56.4 | 36.5 (at 50°C) | 55 |
| *Af*IDH/*Ec*IDH$_{clasp}$ | 80.0 | 108 (at 65°C)<br>[b] (at 70°C) | 70 |
| *Af*IDH | 98.5[c] | 167 (at 65°C)<br>106 (at 70°C) | ~90 |

[a] Data from Karlström et al. (2005)

[b] 6.2% remaining activity after 5 min of incubation

[c] Data from Steen et al. (2001)

$T_m$ by 4°C corresponding to an increase in $t_{1/2}$ at 50°C and a slightly increased $T_{opt}$ (Table 4). Taken together, these data indicate that the inter-domain ionic network in *Af*IDH contributes more to the thermal stability of the native enzyme than the aromatic cluster and the loop-shortening. Interestingly, disruption of an aromatic cluster in *Tm*IDH reduced the apparent $T_m$ by 3.5°C (Karlström et al. 2006), a result comparable with the increased $T_m$ for *Ec*IDH/*Af*IDH$_{clasp}$.

It should be noted that the mutations performed by domain-swapping involve several amino acids and could lead to both favourable and unfavourable interactions with other parts of the enzyme. However, amino acids from both subunits in the dimer contribute to the binding of substrate, allowing any major differences in $k_{cat}$, as a control of conformational changes between wild-type and chimeric enzymes, to be easily detected. Kinetic properties (Table 5) revealed that swapping of the clasp domains did not have a significant effect on the affinities for substrates of the chimers compared to their respective wild-type proteins. Furthermore, catalytic efficiencies ($k_{cat}/K_m$) of the chimers were similar to those determined for wild-type proteins, suggesting that no major conformational changes had occurred upon folding (Table 5). Hence, changes in apparent $T_m$ of the chimers may thus be related to the differences in the clasp domain between *Af*IDH and *Ec*IDH.

## Comparison of heat adaptive traits in hyperthermophilic IDHs

Previously, we have shown that *Af*IDH has a $T_m$ of 98.5°C (Steen et al. 2001) which is similar to the $T_m$ of *Tm*IDH (98.3°C) (Steen et al. 2001) but lower than the one determined for *Ap*IDH (109.9°C) (Steen et al. 2001). Recently, we have succeeded in determining the three-dimensional structure of *Ap*IDH (Karlström et al. 2005) and *Tm*IDH (Karlström et al. 2006). An important factor contributing to the thermal stability of *Ap*IDH was a disulphide bond at the N-terminus of each subunit between Cys9 and Cys87. *Af*IDH lacks the distinct N-terminal extension involved in formation of this disulphide bound in *Ap*IDH and only one cysteine residue was observed in each subunit of the *Af*IDH structure. Hence, no disulphide bridges could be identified in the *Af*IDH structure. The *Tm*IDH has a shorter primary sequence than *Af*IDH (412) and *Ap*IDH (435) with 399 amino acids. Furthermore, as described above for the *Af*IDH, the inter-subunit assembly in the clasp domain is different in the *Tm*IDH from subfamily II compared to the IDHs in subfamily I (Karlström et al. 2006). The difference is also evident in the location of the C- and N-terminal in the structure from *Tm*IDH where the side chains in the two termini are separated by a distance of 4.2 Å (Karlström et al. 2006), whereas in *Af*IDH, *Ap*IDH and *Ec*IDH from subfamily I the termini are separated on the large domain by 40, 42.7 and 41.5 Å, respectively (subunit A). Stabilization of the N-terminus was seen in the structure from *Tm*IDH by electrostatic compensation between three lysines (3, 5 and 7) and two aspartic acid residues (36 and 341). In the structure from *Tm*IDH an ionic interaction between Asp389,

**Table 5** Kinetics of chimers and wild-type enzymes

| Enzyme | kDa | $K_m$ (μM) | | $k_{cat}$ ($s^{-1}$)[a] | | $k_{cat}/K_m$ ($\mu M^{-1}$ $s^{-1}$) | |
|---|---|---|---|---|---|---|---|
| | | Isocitrate | $NADP^+$ | Isocitrate | $NADP^+$ | Isocitrate | $NADP^+$ |
| *Ec*IDH | 45.8 | 40.5 | 39.2 | 106.3 | 88.1 | 2.6 | 2.2 |
| *Ec*IDH/*Af*IDH$_{clasp}$ | 45.4 | 26.1 | 56.8 | 71.7 | 86.6 | 2.7 | 1.5 |
| *Af*IDH/*Ec*IDH$_{clasp}$ | 46.2 | 519 | 15.7 | 219.0 | 155.1 | 0.4 | 9.8 |
| *Af*IDH | 45.8 | 332 | 16.5 | 254.6 | 219.3 | 0.7 | 13.3 |

Kinetic parameters were determined at 40°C (wild-type *Ec*IDH and *Ec*IDH/*Af*IDH$_{clasp}$) or 60°C (wild-type *Af*IDH and *Af*IDH/*Ec*IDH$_{clasp}$)

[a] Per catalytic site

located on a helix in the C-terminus, and Lys29 (close to N-terminus), was found to be important for the stability of the protein. Site-directed mutagenesis resulted in a considerable decrease in apparent $T_m$ of almost 22°C compared to the recombinant wild-type of *Tm*IDH (Karlström et al. 2006). The ionic interaction was also shown to be conserved in *Pc*IDH and *Hc*IDH and due to the high impact of the mutation in *Tm*IDH, believed to be involved in the protection of both termini from thermal unfolding. As described above, an aromatic cluster was observed in the N-terminal region of *Af*IDH and is most likely an alternative strategy for this protein to protect the flexible region of the N-terminus from heat degradation. Furthermore, an ionic interaction was observed in the N-terminus of *Af*IDH between Lys14 and Glu90 (helix *c*), however, this interaction was also found to be conserved in *Ec*IDH. In the C-terminus no ionic interaction was observed in *Af*IDH or *Ec*IDH at 4.0 Å cut off, however, at 6.0 Å a four-membered ionic network was observed in *Af*IDH involving Arg48 (helix *a*), Glu403 (helix *m*), Arg399, (helix *m*) and Glu400 (helix *m*) (subunit B). Ionic interactions in the N-and C-terminus to prevent heat denaturation have also been observed in studies from other hyperthermophilic proteins, in particular the extensive work performed on citrate synthase (Bell et al. 2002).

In *Ap*IDH, more ion pairs and larger ionic networks were present in the protein contra the mesophilic *Ec*IDH homolog. A major determinant conferring the increased thermal stability in *Ap*IDH, confirmed by mutational studies was a seven-membered inter-domain ionic network with many neighbouring charged residues extending the network to 23 members if a cut off of 6 Å instead of 4.2 Å was used. In *Af*IDH only three of these seven amino acid residues were conserved. In the structure of *Tm*IDH no inter-domain ionic networks were identified (Karlström et al. 2006).

As previously found for *Ap*IDH, *Af*IDH contained a small number of inter-subunit ion pairs. At 4.0 Å distance cut off, only four inter-subunit ion pairs were found in *Af*IDH (between Arg163 in the clasp domain and Glu196 from the small domain from both subunits, and the conserved interaction between Lys233 and Asp301 in each active site). There were no differences in the number of inter-subunit ion pairs when compared to the mesophilic *Ec*IDH, which also contained four inter-subunit ion pairs at 4.0 Å. Increasing the cut off to 6.0 Å did not reveal any major differences in the number of inter-subunit ion pairs in the hyperthermophilic *Ap*IDH and *Af*IDH compared to the mesophilic *Ec*IDH (12, 11 and 10 ion pairs, respectively). In contrast, *Tm*IDH was found to have more inter subunit ion pairs than its mesophilic counterparts (Karlström et al. 2006).

In conclusion, the structural comparison between the three hyperthermophilic IDH homologs has revealed the importance of stabilization of the N-terminus, although different strategies have been employed by the different enzymes. The size and positioning of ionic networks differs among the model enzymes, a result in common with previous observations for hyperthermophilic glutamate dehydrogenases (GDH) (Britton et al. 1999; Bhuiya et al. 2005). As may be expected from the exceptional high $T_m$ of *Ap*IDH, this enzyme has larger networks compared with both *Tm*IDH and *Af*IDH. The importance of electrostatic contribution to the stability of hyperthermophilic proteins has previously been discussed by Xiao and Honig (1999). Their study revealed that in all instances the electrostatic interactions were more favourable in the hyperthermophilic proteins compared to mesophilic homologs. Furthermore, the electrostatic free energy was found not to be correlated with the number of ionisable amino acids, ion pairs or ion pair networks in a protein structure, but rather the location of these groups within the structure. It has previously been noted that each of the hyperthermophilic IDHs under investigation have net charges towards zero as opposed to mesophilic *Ec*IDH and porcine IDH. Furthermore, when the cut off was increased to 6 and 8 Å the ionic networks were substantially increased in *Ap*IDH, indicating an electrostatic optimization of the surface (Karlström et al. 2005). In common with *Tm*IDH this was not observed for *Af*IDH, indicating a less optimized surface in these enzymes. It should be noted that the $T_m$ of both *Tm*IDH and *Af*IDH is ~10°C lower than that of *Ap*IDH.

**Acknowledgments** This work was supported by the Norwegian Research Council (Project no. 153774/420). The Norwegian Structural Biology Centre (NorStruct) is supported by the national Functional Genomics Programme (FUGE) of the Research Council of Norway. Provision of beamtime at the Swiss Light Source is gratefully acknowledged. We are grateful to Prof. Aurora Martinez, Department of Biomedicine, University of Bergen, for access to her laboratory facilities and expertise in use of differential scanning calorimetry. The excellent laboratory skills of Lisbeth Glærum and Marit Steine Madsen are also much appreciated.

## References

Bell GS, Russell RJM, Connaris H, Hough DW, Danson MJ, Taylor GL (2002) Stepwise adaptations of citrate synthase to survival at life's extremes. From psychrophile to hyperthermophile. Eur J Biochem 269:6250–6260

Bhuiya MW, Sakuraba H, Ohshima T, Imagawa T, Katunuma N, Tsuge H (2005) The first crystal structure of hyperthermostable NAD-dependent glutamate dehydrogenase from *Pyrobaculum islandicum*. J Mol Biol 345:325–337

Blöchl E, Burggraf S, Fiala G, Lauerer G, Huber G, Huber R, Rachel R, Segerer A, Stetter KO, Völkl P (1995) Isolation, taxonomy and phylogeny of hyperthermophilic microorganisms. World J Microbiol Biotechnol 11:9–16

Bradford MM (1976) A rapid and sensitive method for the quantification of microgram quantities of protein utilizing the principle of protein-dye binding. Anal Biochem 7:248–254

Britton KL, Yip KSP, Sedelnikova SE, Stillman TJ, Adams MWW, Ma K, Maeder DL, Robb FT, Tolliday N, Vetriani C (1999) Structure determination of the glutamate dehydrogenase from the hyperthermophile *Thermococcus litoralis* and its comparison with that from *Pyrococcus furiosus*. J Mol Biol 293:1121–1132

Cary SC, Shank T, Stein J (1998) Worms bask in extreme temperatures. Nature 391:545–546

CCP4 (1994) The CCP4 suite: programs for protein crystallography. Acta Crystallogr D Biol Crystallogr 50:760–763

Ceccarelli C, Grodsky NB, Ariyaratne N, Colman RF, Bahnson BJ (2002) Crystal structure of Porcine mitochondrial $NADP^+$-dependent isocitrate dehydrogenase complexed with $Mn^{2+}$ and isocitrate. Insights into the enzyme mechanism. J Biol Chem 277:43454–43462

Dalhus B, Saarinen M, Sauer UH, Eklund P, Johansson K, Karlsson A, Ramaswamy S, Bjork A, Synstad B, Naterstad K (2002) Structural basis for thermophilic protein stability: structures of thermophilic and mesophilic malate dehydrogenases. J Mol Biol 318:707–721

Dean AM, Koshland DE Jr (1993) Kinetic mechanism of *Escherichia coli* isocitrate dehydrogenase. Biochemistry 32:9302–9309

Fiala G, Stetter KO (1986) *Pyrococcus furiosus* sp. nov. represents a novel genus of marine heterotrophic archaebacteria growing optimally at 100°C. Arch Microbiol 145:56–61

Gouet P, Courcelle E, Stuart DI, Metoz F (1999) ESPript: analysis of multiple sequence alignments in postscript. Bioinformatics 15:305–308

Huber R, Langworthy TA, König H, Thomm M, Woese CR, Sleytr UB, Stetter KO (1986) *Thermotoga maritima* sp. nov. represents a new genus of unique extremely thermophilic eubacteria growing up to 90°C. Arch Microbiol 144:324–333

Hurley JH, Thorsness PE, Ramalingam V, Helmers NH, Koshland DEJ, Stroud RM (1989) Structure of a bacterial enzyme regulated by phosphorylation, isocitrate dehydrogenase. Proc Natl Acad Sci USA 86:8635–8639

Jones TA, Zou JY, Cowan SW, Kjeldgaard M (1991) Improved methods for building protein models in electron-density maps and the location of errors in these models. Acta Crystallogr A 47:110–119

Kabsch W, Sander C (1983) Dictionary of protein secondary structure: pattern recognition of hydrogen-bonded and geometrical features. Biopolymers 22:2577–2637

Kannan N, Vishveshwara S (2000) Aromatic clusters: a determinant of thermal stability of thermophilic proteins. Protein Eng 13:753–761

Karlström M, Stokke R, Steen IH, Birkeland NK, Ladenstein R (2005) Isocitrate dehydrogenase from the hyperthermophile *Aeropyrum pernix*: X-ray structure analysis of a ternary enzyme-substrate complex and thermal stability. J Mol Biol 345:559–577

Karlström M, Steen IH, Madern D, Fedoy AE, Birkeland NK, Ladenstein R (2006) The crystal structure of a hyperthermostable subfamily II isocitrate dehydrogenase from *Thermotoga maritima*. FEBS J 273:2851–2868

Karshikoff A, Ladenstein R (2001) Ion pairs and the thermotolerance of proteins from hyperthermophiles: a 'traffic rule' for hot roads. Trends Biochem Sci 26:550–556

Knapp S, de Vos WM, Rice D, Ladenstein R (1997) Crystal structure of glutamate dehydrogenase from the hyperthermophilic eubacterium *Thermotoga maritima* at 3.0 A resolution. J Mol Biol 267:916–932

Leslie AGW (1992) Joint CCP4 and ESF-EACMB. Newslett Protein Crystallogr 27–33

Murshudov GN, Vagin AA, Lebedev A, Wilson KS, Dodson EJ (1999) Efficient anisotropic refinement of macromolecular structures using FFT. Acta Crystallogr D Biol Crystallogr 55:247–255

PyMol (2005) DeLano Scientific, 0.98 ed, California, USA

Russell RB, Barton GJ (1992) Multiple protein sequence alignment from tertiary structure comparison: assignment of global and residue confidence levels. Proteins 14:309–323

Sako Y, Nomura N, Uchida A, Ishida Y, Morii H, Koga Y, Hoaki T, Maruyama T (1996) *Aeropyrum pernix* gen. nov., sp. nov., a novel aerobic hyperthermophilic archaeon growing at temperatures up to 100 degrees C. Int J Syst Bacteriol 46:1070–1077

Scandurra R, Consalvi V, Chiaraluce R, Politi L, Engel PC (2000) Protein stability in extremophilic archaea. Front Biosci 5:d787–d795

Singh SK, Matsuno K, LaPorte DC, Banaszak LJ (2001) Crystal structure of *Bacillus subtilis* isocitrate dehydrogenase at 1.55 Å. Insights into the nature of substrate specificity exhibited by *Escherichia coli* isocitrate dehydrogenase kinase/phosphatase. J Biol Chem 276:26154–26163

Spassov VZ, Ladenstein R, Karshikoff AD (1997) Optimization of the electrostatic interactions between ionized groups and peptide dipoles in proteins. Protein Sci 6:1190–1196

Steen IH, Lien T, Birkeland NK (1997) Biochemical and phylogenetic characterization of isocitrate dehydrogenase from a hyperthermophilic archaeon, *Archaeoglobus fulgidus*. Arch Microbiol 168:412–420

Steen IH, Madern D, Karlström M, Lien T, Ladenstein R, Birkeland NK (2001) Comparison of isocitrate dehydrogenase from three hyperthermophiles reveals differences in thermostability, cofactor specificity, oligomeric state, and phylogenetic affiliation. J Biol Chem 276:43924–43931

Stetter KO (1999) Extremophiles and their adaptation to hot environments. FEBS Lett 452:22–25

Stoddard BL, Dean A, Koshland DE (1993) Structure of isocitrate dehydrogenase with isocitrate, nicotinamide adenine-dinucleotide phosphate, and calcium at 2.5 Å resolution: a pseudo-michaelis ternary complex. Biochemistry 32:9310–9316

Vetriani C, Maeder DL, Tolliday N, Yip KSP, Stillman TJ, Britton KL, Rice DW, Klump HH, Robb FT (1998) Protein thermostability above 100°C: a key role for ionic interactions. Proc Natl Acad Sci USA 95:12300–12305

Vieille C, Zeikus GJ (2001) Hyperthermophilic enzymes: sources, uses, andmolecular mechanisms for thermostability. Microbiol Mol Biol Rev 65:1–43

Warrens AN, Jones MD, Lechler RI (1997) Splicing by overlap extension by PCR using asymmetric amplification: an improved technique for the generation of hybrid proteins of immunological interest. Gene 186:29–35

Xiao L, Honig B (1999) Electrostatic contributions to the stability of hyperthermophilic proteins. J Mol Biol 289:1435–1444

Xu X, Zhao J, Xu Z, Peng B, Huang Q, Arnold E, Ding J (2004) Structures of human cytosolic NADP-dependent isocitrate dehydrogenase reveal a novel self-regulatory mechanism of activity. J Biol Chem 279:33946–33957

Yip K, Stillman T, Britton K, Artymiuk P, Baker P, Sedelnikova S, Engel P, Pasquo A, Chiaraluce R, Consalvi V (1995) The structure of *Pyrococcus furiosus* glutamate dehydrogenase reveals a key role for ion-pair networks in maintaining enzyme stability at extreme temperatures. Structure 3:1147–1158

Yip KSP, Britton KL, Stillman TJ, Lebbink J, de Vos WM, Robb FT, Vetriani C, Maeder D, Rice DW (1998) Insights into the molecular basis of thermal stability from the analysis of ion-pair networks in the glutamate dehydrogenase family. Eur J Biochem 255:336–346